

Article

Chemical Characteristics of Zirconium Chloride and Zirconium Oxide Nanoparticles Driving Toxicity on *Lemna minor*

Mohamadou Diallo  and David Dewez * 

Laboratory of Environmental & Analytical Biochemistry of Contaminants, Nanoqam, Department of Chemistry, University of Quebec at Montreal, C.P. 8888, succ. Centre-ville, Montreal, QC H3C 3P8, Canada; diallo.mohamadou@courrier.uqam.ca

* Correspondence: dewez.david@uqam.ca; Tel.: +1-514-987-3000 (ext. 3278)

Abstract: The increasing global production and utilization of zirconium (Zr) compounds, including zirconium chloride ($ZrCl_4$) and zirconium oxide nanoparticles (NPs- ZrO_2), raises concerns about their potential environmental impact. This study investigated the toxicity mechanisms of $ZrCl_4$ and NPs- ZrO_2 on the aquatic plant *Lemna minor*. The physicochemical properties of NPs- ZrO_2 in the test medium were characterized, revealing concentration-dependent changes in the hydrodynamic diameter, zeta potential, and solubility over time. The analysis of Zr speciation showed the predominance of $Zr(OH)_4(aq)$ species from $ZrCl_4$. Plants of *L. minor* exposed to $ZrCl_4$ and NPs- ZrO_2 exhibited differential Zr bioaccumulation, growth inhibition, oxidative stress, and antioxidant responses. $ZrCl_4$ induced a higher toxicity than NPs- ZrO_2 , with bioaccumulation strongly correlating with adverse effects. The differential toxicity impact between these two Zr-compounds was also determined by the lowest observed-effect doses for growth and biochemical parameters. The scanning electron microscopy coupled with energy-dispersive X-ray spectroscopy confirmed internalization of NPs- ZrO_2 and Zr uptake in the *L. minor* plant. Therefore, these findings highlighted the importance of chemical speciation, environmental transformations, and biological responses in assessing the ecological impact of Zr-compounds for effective risk assessment and management strategies for protecting aquatic ecosystems.

Keywords: zirconium chloride; zirconium oxide nanoparticles; physicochemical properties; bioavailability; toxicity; biological responses; *Lemna minor*



Citation: Diallo, M.; Dewez, D.

Chemical Characteristics of Zirconium Chloride and Zirconium Oxide Nanoparticles Driving Toxicity on *Lemna minor*. *Environments* **2024**, *11*, 222. <https://doi.org/10.3390/environments11100222>

Academic Editor: Chien-Sen Liao

Received: 21 August 2024

Revised: 26 September 2024

Accepted: 5 October 2024

Published: 12 October 2024



Copyright: © 2024 by the authors. Licensee MDPI, Basel, Switzerland. This article is an open access article distributed under the terms and conditions of the Creative Commons Attribution (CC BY) license (<https://creativecommons.org/licenses/by/4.0/>).

1. Introduction

Global Zirconium (Zr) production, primarily sourced from the mineral zircon ($ZrSiO_4$), has reached an estimated 1.4 thousand metric tons (gross weight) in 2022, which is attributed to the escalating demand for zirconium in diverse chemical forms, driven by its applications across various industries [1]. Projections based on the substantial reserves of Zr minerals indicate a further increase in production in the coming years. ZrO_2 accounts for 97% of Zr utilization and is primarily employed in the production of ceramics, chemicals, and synthesized nanomaterials. The metallic form of Zr constitutes about 3% of consumption, with two-thirds dedicated to the nuclear industry for alloy and superalloy production, and one-third allocated to the aeronautics, electronics, electricity, and chemical sectors [2–4]. As it is resistant to corrosion, radiation, and high temperatures, Zr plays a crucial role in the nuclear industry in the manufacturing of fuel grains for uranium oxide pellets, and the addition of pure Zr to alloying elements can enhance the mechanical properties of fuel grains in nuclear reactors [3,4]. As the nuclear industry expands, the importance of Zr in ceramics is growing, and we can anticipate an increased demand in the foreseeable future. However, information on the specific environmental impacts of Zr production and use is limited at the user level, and the secure storage of nuclear waste, including spent fuel and compacted grains, presents significant challenges in assessing long-term contamination risks [5].

Zirconium (IV) chloride, also known as zirconium tetrachloride ($ZrCl_4$), is a precursor to various other Zr-compounds that play a crucial role in the conversion of minerals from zirconium-to-zirconium metals through the Kroll process [6]. In laboratories of organic synthesis, $ZrCl_4$ acts as a weak Lewis acid, finding applications in the Friedel–Crafts reaction, the Diels–Alder reaction, and intramolecular cyclization reactions [7]. Despite its utility, it is known that $ZrCl_4$ exhibits a low toxicity, with median lethal dose values (LD_{50}) of 440 mg/kg and 1688 mg/kg reported in mice and rats, respectively [8,9]. This low toxicity profile allows for the use of $ZrCl_4$ as a Lewis acid in various organic transformations, aligning with the principles of green chemistry [8]. Notably, it serves as a safer alternative to traditional Lewis acids that are harmful to mammals, such as aluminum chloride ($AlCl_3$) and boron trifluoride (BF_3). Previous studies on soil–plant systems (e.g., *Hordeum vulgare*, *Triticum aestivum*) had reported Zr sequestration in roots and Zr-induced toxicity in plant cells, indicated by a marked decrease in total phenol content of plant tissues and alterations in enzyme activities (peroxidase, ascorbate peroxidase and glutathione reductase), which were associated with the plant response to different stress conditions [10]. These studies highlighted the importance of understanding Zr behavior in soil–plant systems, along with its potential mobility and impact on ecosystems. A recent study by Madany et al. (2023) [11] conducted on oat plants (*Avena sativa*) demonstrated that Zr contamination caused a significant diminution of plant biomass and photosynthetic efficiency by triggering oxidative damage. The authors showed that elevated levels of CO_2 mitigated the adverse effects of Zr on plant growth and redox homeostasis. In an aquatic environment, Zr salts can exhibit potential coagulant properties, enhancing purification efficiency and forming bioinert Zr-oxyhydroxide precipitates [12]. $ZrCl_4$, due to its high affinity for phosphorus, has been identified as a significant player in water treatment, surpassing other metals like aluminum in the removal of phosphorus, suspended solids, and turbidity. However, Zr-phosphates were formed during the water purification processes, which persisted and bioaccumulated in aquatic organisms [12]. Moreover, Caroline et al. (2019) [13] showed that exposure to environmental concentrations of Zr affected the micrometazoan structure of biofilms and modified the autotrophic biofilm structure by increasing the proportion of green algae and decreasing the abundance of cyanobacteria and brown algae, indicating a toxic effect of Zr on rotifers and potential indirect effects on micrometazoan community structures. The study also found that rotifers and the ciliate *Aspidisca cicada* appeared to be the most sensitive organisms to Zr exposure, indicating potential impacts on the biodiversity of aquatic ecosystems. However, the information is limited specifically on the toxicity mechanisms of $ZrCl_4$ with respect to aquatic organisms, and further research is needed to provide a comprehensive understanding of its toxicological properties.

Various synthesis methods, including sol-gel and forced hydrolysis, are employed in the production of zirconium oxide nanoparticles (NPs- ZrO_2). These methods offer the advantage of controlling physicochemical properties such as nanoparticle size, structure, and composition [14,15]. Due to its antimicrobial properties, NPs- ZrO_2 are extensively utilized in various nanoactivated products, including ceramics, pharmaceuticals, medical devices, and oxygen sensors [16]. Additionally, ZrO_2 serves as an effective thermal insulator in gas turbine manufacturing, safeguarding metal parts by limiting heat transfer [17]. In the field of electronics, ZrO_2 acts as an excellent electrical insulator, finding applications in the production of transistors and storage memories [18,19]. In the field of medicine, ZrO_2 is widely employed in the fabrication of ceramic dental prostheses, owing to its commendable mechanical properties, biocompatibility, and durability [20]. The increasing industrialization and global market demand are expected to drive a surge in production of NPs- ZrO_2 , inevitably leading to the emission of these nanoparticles into the environment [21]. Similarly to other metal oxide nanoparticles, ZrO_2 has demonstrated antimicrobial activity on the biofilm formation of *Streptococcus mutans*, *Staphylococcus aureus*, and *Klebsiella pneumoniae* [22,23]. In the case of soil invertebrates, in vitro studies using *Enchytraeus crypticus* demonstrated absorption of NPs- ZrO_2 by cells, without notable changes in antioxidant stress levels or cell viability [24]. In vitro studies on HepG2 cell lines have indicated the

genotoxic and cytotoxic effects of NPs-ZrO₂, although conflicting results have been reported for MDA-MB-231 cell lines, where no cytotoxicity was observed [23,24]. In vivo analysis data from mice exposed to an intravenous injection of 20 mg/kg of NPs-ZrO₂ showed an accumulation in the body, with minimal reproductive effects [24]. A recent study on freshwater alga *Scenedesmus obliquus* exposed to NPs-ZrO₂ (1 mg/L) reported a significant increase in lipid peroxidation products, antioxidant small molecule metabolites, and the enzyme activity of Superoxide Dismutase [25]. The toxicity of NPs-ZrO₂ was found in aquatic crustaceans, where it caused their immobilization and altering enzymatic activities. Furthermore, chronic tests with protozoans showed that NPs-ZrO₂ had a harmful effect, with a significant impact on growth and reproduction [26]. These few studies indicated the potential accumulation and toxicity risk of NPs-ZrO₂ on different organisms, but further research is needed to fully understand their toxicological effects. It is essential for proper Zr-containing waste management practices to prevent the impact of the continuous release of Zr into terrestrial and aquatic compartments.

The potential ecological impacts of Zr contamination are still an area of concern, which may have implications at higher trophic levels. The toxicity mechanisms of Zr-compounds represent an important subject of investigation, since the chemical composition and specific form of Zr (ionic vs. particulate) will determine its environmental impact. Here, we studied the mechanisms of Zr toxicity associated with ZrCl₄ and NPs-ZrO₂, utilizing the aquatic plant *Lemna minor* as a convenient model organism for bioassay toxicity testing. The biological responses of this plant to trace metals exposure can imply several biomarkers, which can be used for toxicity assessment and phytoremediation [27–29], highlighting the importance of using *Lemna* plants in environmental monitoring and risk assessment [30–32]. To compare ZrCl₄ and NPs-ZrO₂, we characterized their physicochemical properties in the tested aqueous medium and assessed their accumulation within the plant biomass. Growth and biochemical biomarkers were employed to characterize their toxic effects on plant physiology, providing a comprehensive understanding of the impact of ZrCl₄ and NPs-ZrO₂ on the plant. The environmental significance of the studied Zr-compounds will be discussed with respect to their potential ecological impacts.

2. Materials and Methods

2.1. Physicochemical Characterizations of Zirconium Oxide Nanoparticles

The NPs-ZrO₂ were characterized using Transmission Electron Microscopy (TEM) and Energy Dispersive X-ray Spectroscopy (EDS) (Figure S1), confirming the ZrO₂ composition, showing the nanoparticles spherical morphology and size range (approximately 10–20 nm in diameter), and the dispersion and agglomeration state of nanoparticles in the medium. These characterizations informed about the nanoparticles before and after dissolution in the medium, suggesting potential interactions or surface modifications of the nanoparticles. The X-ray diffraction (XRD) analysis of NPs-ZrO₂ was done to provide information about the sample crystallite size and structural properties (Figure S2). The XRD pattern provided the crystalline nature of the NPs-ZrO₂, indicating the presence of both monoclinic and tetragonal phases. The Raman spectrum of NPs-ZrO₂ was determined, showing distinct peaks corresponding to the vibrational modes of both monoclinic and tetragonal phases of zirconium dioxide (Figure S3). The presence of multiple Bg and Ag modes indicated a mixture of these phases, with the specific peak positions and intensities providing detailed information about the crystalline structure and phase composition of the nanoparticles. The FT-IR (Fourier Transform Infrared) spectrum of NPs-ZrO₂ (Figure S4), revealed the presence of surface hydroxyl groups, the adsorbed water molecules, and the characteristic Zr-O bonds.

2.2. Preparation of ZrCl₄ and Stock Solutions of NPs-ZrO₂

The ZrCl₄ utilized in this study, having a purity of 99.9%, was procured from Sigma-Aldrich (Product No.357405, CAS No.10026-11-6, Saint Louis, MO, USA) and a stock solution with a concentration of 20 mg/mL was prepared in Nanopure-purified water. The

resultant stock solution underwent 30 min of sonication at room temperature and was subsequently stored at 4 °C for later use [15]. The powder of NPs-ZrO₂ was acquired from Sigma-Aldrich (Product No.544760, CAS No.1314-23-4, Saint Louis, MO, USA), and the size distribution of particles was less than or equal to 100 nm with a surface area of 25 m²/g or more. The stock suspension of these nanoparticles was created by dispersing the powder in Nanopure-purified water. Nanopure-purified water was provided using a Milli-Q water purification system (Merck KGaA, Darmstadt, Germany) with the following specifications: resistivity of 18.2 MΩ·cm and total organic carbon ≤ 5 ppb. Following 30 min of sonication in a sonication bath at room temperature, the suspensions underwent an additional 10 min of ultrasonication using a probe before being stored at 4 °C for future use [15,23].

2.3. Hydrodynamic Diameter and Zeta Potential Analysis of Nanoparticle Suspensions

Hydrodynamic diameter analysis of suspensions of NPs-ZrO₂ at concentrations of 1, 50, 100, 150, and 200 mg/L in the Swedish Standard (SIS) culture medium was conducted on days 0 and 7 using a Zetasizer (Nano ZS90, Malvern Instruments Ltd., Worcestershire, UK). Triplicate measurements were performed for each condition, and each experiment was independently repeated three times. The Zeta potential of NPs-ZrO₂ at various concentrations in the SIS medium was determined using a ZetaPlus instrument (Brookhaven Instruments Corp., Nashua, NH, USA), with data acquisition performed using the Zeta potential analyzer Ver.5.68 software.

2.4. Lemna Minor Plant Growth Conditions

The cultivation of *Lemna minor* plants was conducted using the growing medium established by the Swedish Standard (SIS), following the guidelines outlined in the OECD (Organization for Economic Co-operation and Development) Guidance #221 (2006) [33]. The SIS growth medium comprises various nutrients in mg/L: NaNO 85; KH₂PO₂ 13.4; MgSO₂·7H₂O 75; CaCl₂·2H₂O 36; Na₂CO₃ 20; H₃BO₃ 1; MnCl₂·4H₂O 0.2; Na₂MoO₄·2H₂O 0.01; ZnSO₄·7H₂O 0.05; CuSO₄·5H₂O 0.005; Co(NO₃)₂·6H₂O 0.01; FeCl₃·6H₂O 0.84; Na₂-EDTA·2H₂O 1.4; and MOPS 490. Chemicals were acquired from Sigma-Aldrich (Saint Louis, MO, USA). The pH of the medium was adjusted to 6.5 ± 0.2. Following this, the medium underwent sterilization via filtration through a 0.2 µm filter. The cultures were maintained at a temperature of 24 ± 2 °C, with a photoperiod of 16 h of illumination at a light intensity of 110 ± 25 µmol photons/m²/s, followed by 8 h of darkness. For future use in experiments, a stock culture was regularly maintained for the availability of healthy, young, and growing individual plants of *L. minor* without any lesions or chlorosis.

2.5. Bioassay Toxicity Testing of ZrCl₄ and Concentrations of NPs-ZrO₂

Three individual plants, having two fronds, were exposed during 7 days to increasing nominal concentrations of ZrCl₄ and NPs-ZrO₂ (0, 1, 50, 100, 150, and 200 mg/L), prepared in Erlenmeyer flasks (250 mL) containing 100 mL of axenic SIS culture medium, following OECD recommendations 2006 #221 [33]. This setup permitted the plant roots to be immersed at a depth of 2 cm in the medium and the leaves to have enough air space for gas exchange. The reproducibility of exposure experiments was ensured. All experimental conditions were maintained under the same light and temperature conditions as the stock culture of *L. minor*. Prior to the initiation of the experiment, the different treatment concentrations were thoroughly homogenized and sonicated to prevent precipitation resulting from a high concentration of dissolved metal [15]. All bioanalytical analyses were performed at the day 7 of exposure period.

2.6. Speciation Analysis

To assess the various chemical forms of Zr within the test medium, the speciation was estimated at a temperature of 25 °C utilizing Visual MINTEQ 3.1 chemical equilibrium software (Department of Land and Water Resources Engineering, Royal Institute of Technology KTH). This software tool is designed to model chemical equilibrium in

aqueous systems to predict the behavior of dissolved substances, including speciation, solubility, and interactions between various chemical species. Visual MINTEQ constructs mass balance equations for each element present in the system and includes a wide range of equilibrium reactions such as complexation, precipitation/dissolution, and ion pairing. It also relies on extensive thermodynamic databases that provide necessary parameters like stability constants, solubility products, and activity coefficients. This analysis aimed to identify the distribution of different Zr chemical species in the SIS growth medium.

2.7. Assessment of Lemna Minor Growth

The average specific population growth rate based on the dry weight of the plants was calculated for each test condition, following the formula recommended by OECD guidelines 2006 #221 [33]:

$$\mu_{i-j} = [\ln(N_j) - \ln(N_i)]/7 \quad (1)$$

In this formula, μ_{i-j} represents the average specific growth rate from i to j , where N is the measure of the variable for each condition at time i (day 0) and j (day 7), and t is the elapsed time from i to j (7 days).

Additionally, the growth inhibition rate (Ir) was calculated as a percentage using the following formula:

$$Ir = [(\mu_C - \mu_T)/\mu_C] \times 100 \quad (2)$$

The variables μ_C and μ_T represent the specific growth rate for the control and treatment conditions, respectively. These calculations enable the assessment of the impact of different experimental conditions on the growth rate and the estimation of the degree of growth inhibition compared to the control.

2.8. Zirconium Content in Plant Biomass

The determination of Zr content in plant biomass for all experimental conditions involved several steps. After harvesting, the plants underwent a thorough wash with EDTA to eliminate any traces of metal and nanoparticles from the plant surface. Subsequently, the plants were dehydrated in an oven at 60 °C for 15 h, and the dry weight was measured (at weight constant USP731). The samples were then homogenized in the dark using a mortar and pestle, along with 2 mL of Nanopure-purified water and Ottawa sand. For biomass digestion, the homogenates were digested in 2 mL of 70% HNO₃ in a sand bath at 90 °C for 6 h, until the acid completely evaporated. The residues obtained were solubilized with 5 mL of 5% HNO₃ for 16 h, before the analysis by optical plasma emission spectrometry (ICP-OES 5100, Agilent Technologies Canada Inc., Mississauga, ON, Canada). The obtained values were normalized per mass unit as µg of Zr/mg of dry mass (DM).

2.9. Quantifying Glutathione Levels in Plant

The cellular level of reduced glutathione (GSH) was assessed using the violet Thiol Tracker fluorescent probe (Product no.T10095, ThermoFisher Scientific, Waltham, MA, USA), as previously described [34]. The Thiol Tracker solution was prepared by dissolving the violet Thiol Tracker in DMSO and then diluting it in saline phosphate buffer (PBS) to achieve a concentration of 20 µM. Following the treatments, the entire plants (fronds and roots) were arranged in a 96-well plate and incubated with 100 µL of the Thiol Tracker solution for 10 min. Measurements were conducted using a microplate reader, model Tecan Infinite M200, with an excitation wavelength of 405 nm and an emission wavelength of 526 nm.

2.10. Evaluating Reactive Oxygen Species Levels

The level of reactive oxygen species (ROS) was quantified using the green fluorescent probe CellROX (Product no.C10444, ThermoFisher Scientific, Waltham, MA, USA), which binds to DNA after oxidation in the nucleus and mitochondria. Additionally, the orange fluorescent probe CellROX (Product no.C10443, ThermoFisher Scientific, Waltham, MA,

USA) was employed, binding to DNA in the cytoplasm. For each treatment condition, the plants were harvested and incubated for 30 min at 37 °C with 5 µM of these fluorescent reagents. Then, the plants underwent three washes with saline phosphate buffer (PBS) at room temperature. Measurements were conducted using the Tecan Infinite M200 microplate reader (Woburn, MA, USA), with excitation and emission wavelengths of 545/565 nm for the orange CellROX, while excitation and emission wavelengths of 485/520 nm for the green CellROX.

2.11. Microscopic Analysis of Incorporation of Nanoparticles

The analysis of the surface structure and ultrastructure of plants exposed to NPs-ZrO₂ was conducted at the Centre for Materials Characterization (CM2) of École Polytechnique de Montréal. This characterization was performed using a JEOL brand field emission scanning electron microscope (JSM-7600TFF, JEOL Canada Inc., Saint-Hubert, QC, Canada) equipped with an X-Max detector (OXFORD Instruments NanoAnalysis, Concord, MA, USA), featuring a resolution of the order of a micrometer, and coupled to an energy-dispersive X-ray spectrometer (EDS). Before the analysis, the plants underwent drying and fixation on a layer of carbon and were subsequently subjected to maximum vacuum. Deposits were made for 7 min using a coating technique with a Quorum Q150T Plus device (Laughton, East Sussex, UK). This approach enabled the acquisition of high-quality images and the analysis of the chemical composition of the samples at the nanoscale.

2.12. Statistical Analysis

The means and standard deviations were determined for $n = 6$ for all testing conditions. A one-way ANOVA analysis of variance test was performed using GraphPad Prism software version 8.0.2 (Boston, MA, USA). Subsequently, the post-hoc Tukey HSD (Honestly Significant Difference) test was applied to identify significant differences between treatment conditions. In the figures, distinct lowercase letters are utilized to indicate significant differences between conditions, with a significance level set at $p < 0.05$.

3. Results and Discussion

3.1. Properties of Zr-Compounds: Zr Speciation, Bioavailability, Agglomeration, Reactivity, and Stability

The physicochemical properties of NPs-ZrO₂ can affect the hydrodynamic size, agglomeration state, surface reactivity, and solubility of the nanoparticles in SIS medium. The presence of hydroxyl groups and adsorbed water found at the nanoparticles' surface (FT-IR spectrum, Figure S4) could increase their hydrodynamic size by forming a hydration layer around the nanoparticles, which can lead to hydrogen bonding between particles, promoting agglomeration. The Raman spectrum of the NPs-ZrO₂ (Figure S3) confirmed the presence of both monoclinic and tetragonal phases, which can have different surface energies contributing to agglomeration. In addition, the surface reactivity of the NPs-ZrO₂ is significantly influenced by the presence of surface hydroxyl groups by participating in various chemical reactions. The FT-IR spectrum suggests that water molecules are adsorbed on the surface, which can enhance solubility by forming a hydration layer. Therefore, the presence of surface hydroxyl groups and adsorbed water molecules could increase the hydrodynamic size and surface reactivity, while also enhancing solubility. However, the potential for agglomeration existed due to hydrogen bonding and surface interactions.

The speciation of Zr ions in the presence of other chemical species in the SIS culture medium was investigated using Visual MINTEQ software (Table 1). The speciation of free Zr in the SIS medium showed limited availability, as Zr predominantly forms the chemical species Zr(OH)₄(aq) through complexation with hydroxyl (OH) groups. The results revealed that Zr ions predominantly form Zr(OH)₄(aq), which is the main species compared to Zr(OH)₅⁻. This indicates that Zr ions tend to hydrolyze rather than remain in their free ionic form. Consequently, the majority of the Zr that was bioavailable for the plants was in the form of Zr(OH)₄(aq), and this observation aligned with the accumulation

of Zr in the plant biomass observed after a 7-day incubation with $ZrCl_4$ at concentrations ranging from 1 to 200 mg/L. In addition, the limited presence of the $Zr-EDTA(aq)$ complex was observed in the SIS medium, which was correlated with the nominal concentrations of $ZrCl_4$. This suggested that while EDTA played a role in buffering the metal ions, its complex with Zr was not the predominant form. When metal ions were absorbed by the plants in small amounts, the $Zr-EDTA$ complex released them to maintain their free concentration in the medium. From this speciation study, the concentrations of Zr chemical species formed were primarily dependent on the dissolved $ZrCl_4$ concentration, emphasizing the predominance of $Zr(OH)_4(aq)$ and the limited role of $Zr-EDTA(aq)$ in the SIS medium.

Table 1. The soluble fraction of Zirconium (sol. Zr) determined by ICP-OES from the nominal concentrations of $ZrCl_4$ in SIS medium after 24 h. The reported values in mg/L are expressed as averages \pm standard deviation ($n = 6$). For each condition, the estimated chemical species are expressed in % from the total Zr in the soluble fraction.

[$ZrCl_4$] mg/L [Sol. Zr] mg/L	1 0.41 \pm 0.00	50 19.60 \pm 0.02	100 39.82 \pm 0.34	150 58.69 \pm 0.12	200 76.52 \pm 0.28
Zr^{4+} %	0	0	0	0	0
$Zr(OH)_5^-$ %	0	0.1	0.1	0.09	0.08
$Zr(OH)_4(aq)$ %	97.6	99.5	99.6	99.7	99.78
$ZrEDTA(aq)$ %	2.4	0.4	0.3	0.21	0.14

The characterization results revealed a concentration-dependent increase in the average hydrodynamic diameter (HD) of the NPs- ZrO_2 , ranging from 115 nm to 785 nm at day 0 (D0) (Table 2). This increase indicated the formation of larger aggregates at higher concentrations. The large standard deviations in the HD measurements of the suspension of NPs- ZrO_2 are primarily due to the high particle size heterogeneity of the NPs- ZrO_2 powder and the nanoparticle irregular shapes or non-uniform aggregation, resulting in a wide range of particle sizes. The zeta potential (ZP) measurements on D0 showed that the nanoparticles had a moderately negative surface charge, which became slightly more negative with increasing concentrations, ranging from -26.39 mV to -32.52 mV. This also suggested both initial instability and potential aggregation of the nanoparticles. By day 7 (D7), the HD of the suspended NPs- ZrO_2 decreased significantly, ranging from 144 nm to 188 nm, suggesting the sedimentation of larger aggregates and stabilization of the remaining suspended nanoparticles. The ZP values at D7 become more negative, ranging from -34.24 mV to -36.39 mV, suggesting increased electrostatic repulsion and improved dispersion stability over time.

Table 2. The average hydrodynamic diameter (HD) and the Zeta potential (ZP) of the NPs- ZrO_2 as a function of the nominal concentration in SIS medium at a pH of 6.5 during incubation at day 0 (D0) and day 7 (D7).

[NPs- ZrO_2] mg/L	D0		D7	
	HD (nm)	ZP (mV)	HD (nm)	ZP (mV)
1	115 \pm 22	-32.52 ± 1.00	168 \pm 39	-36.39 ± 1.31
50	255 \pm 177	-27.17 ± 0.63	144 \pm 68	-34.24 ± 1.74
100	421 \pm 358	-26.39 ± 0.91	188 \pm 97	-36.29 ± 0.86
150	339 \pm 323	-26.93 ± 0.70	151 \pm 35	-35.98 ± 2.71
200	785 \pm 372	-26.92 ± 0.78	148 \pm 59	-35.38 ± 1.75

Note: The reported values are expressed as averages \pm standard deviation ($n = 6$).

In addition, the solubility data in Table 3 showed that the soluble fraction of Zirconium (sol. Zr) from the NPs- ZrO_2 decreased over the 7-day incubation period. Initially, at D0, the sol. Zr ranged from 0.05 mg/L at 1 mg/L NPs- ZrO_2 to 2.75 mg/L at 100 mg/L NPs- ZrO_2 . Higher initial concentrations lead to more aggregates in suspension, increasing the initial

solubility due to a larger surface area. However, by D7, the sol. Zr had significantly decreased across all concentrations, with values ranging from 0.02 mg/L to 0.49 mg/L. Over time, the sedimentation of larger aggregates and stabilization of smaller particles in suspension could explain the reduced hydrodynamic diameter and solubility. Also, the increase in the negative zeta potential over time (Table 2) enhanced the stability of nanoparticles in suspension. This low sol. Zr from the NPs-ZrO₂ would exhibit a speciation behavior like free Zr from ZrCl₄ (Table 1). Therefore, the results of Tables 2 and 3 highlights the dynamic behavior of the NPs-ZrO₂ in terms of their hydrodynamic diameter, zeta potential, and solubility over time.

Table 3. The soluble fraction of Zirconium (sol. Zr) in mg/L from samples of the NPs-ZrO₂ incubated in SIS medium at day 0 (D0) and day 7 (D7).

[NPs-ZrO ₂] mg/L	[sol. Zr] mg/L	
	D0	D7
1	0.05 ± 0.00	0.02 ± 0.00
50	1.38 ± 0.06	0.25 ± 0.01
100	2.75 ± 0.07	0.22 ± 0.01
150	0.91 ± 0.01	0.49 ± 0.01
200	1.05 ± 0.01	0.06 ± 0.01

Note: The reported values are expressed as averages ± standard deviation (n = 6).

These data are essential for toxicological assessments as they provide detailed information on the complex relationships between particles agglomeration, surface charge, and solubility, for understanding the behavior of NPs-ZrO₂ in SIS medium. These characteristics directly influence the bioavailability and potential toxicity of nanoparticles, making them crucial for accurate and comprehensive toxicological evaluations. Previous studies have shown that physicochemical properties such as the stability, size, shape, and charge of metal oxide nanoparticles greatly influence their bioavailability and toxicity in aquatic environments [35–38]. Therefore, investigating the conditions of the culture medium is crucial for toxicological evaluations to determine whether changes in the physicochemical properties of NPs-ZrO₂ can influence the mechanisms of toxicity of nanoparticles suspended in aqueous solution. Understanding these parameters helps in predicting the interactions of nanoparticles with biological systems, thereby aiding in effective risk assessment strategies.

3.2. Toxicity of Zirconium Accumulation in *Lemna Minor*: Insights from Exposure Studies with ZrCl₄ and NPs-ZrO₂

The impact of ZrCl₄ and NPs-ZrO₂ on various biological parameters in *Lemna minor* provides valuable insights into their toxic effects on this aquatic plant. Analyzing the growth rate, antioxidant defense mechanisms, reactive oxygen species (ROS) levels, and chlorophyll pigments revealed the plant stress physiological responses. The results are presented in the Table 4, demonstrating that both ZrCl₄ and NPs-ZrO₂ adversely affected *L. minor* plants. The bioaccumulation increased with increasing ZrCl₄ concentrations but remained low for the NPs-ZrO₂, and ZrCl₄ exposure led to significantly higher Zr bioaccumulation compared to the NPs-ZrO₂ at all concentrations. Both ZrCl₄ and NPs-ZrO₂ caused concentration-dependent decreases in the biomass and specific growth rate. Exposure to ZrCl₄ had a more pronounced effect, causing significant growth inhibition at ≥50 mg/L, while the NPs-ZrO₂ only caused significant inhibition at ≥100 mg/L. Cytoplasmic and organelle ROS levels increased with increasing concentrations of both ZrCl₄ and NPs-ZrO₂, indicating the induction of oxidative stress. The results showed that ZrCl₄ generally induced higher ROS levels than the NPs-ZrO₂ at the same concentrations. As an antioxidant response, the total thiol levels increased with increasing concentrations of both ZrCl₄ and the NPs-ZrO₂, but exposure to the NPs-ZrO₂ led to a more pronounced increase in the total thiols compared to ZrCl₄. Overall, ZrCl₄ exposure resulted in a higher bioaccumulation of Zr in plants, with a stronger oxidative stress, and a more severe effect on plant growth.

Table 4. Change in biological parameters of *Lemna minor* plants after 7 days of exposure to different nominal concentrations of ZrCl₄ and NPs-ZrO₂.

Concentration mg/L	ZrCl ₄ NPs-ZrO ₂	Control	1	50	100	150	200
Bioaccumulation µg Zr/mg DW	ZrCl ₄	0.00 ± 0.00 ^a	0.11 ± 0.05 ^a	2.86 ± 0.68 ^a	6.50 ± 0.77 ^b	13.63 ± 1.79 ^c	14.89 ± 0.40 ^d
	NPs-ZrO ₂	0.00 ± 0.00 ^a	0.01 ± 10 ^{-4a}	0.03 ± 10 ^{-3a}	0.01 ± 10 ^{-4a}	0.02 ± 10 ^{-4a}	0.04 ± 10 ^{-4a}
Biomass mg DW	ZrCl ₄	11.07 ± 0.03 ^a	10.99 ± 0.09 ^a	10.54 ± 0.09 ^a	6.15 ± 0.40 ^b	4.10 ± 0.10 ^c	3.41 ± 0.11 ^d
	NPs-ZrO ₂	11.07 ± 0.03 ^a	10.85 ± 0.03 ^a	10.67 ± 0.11 ^a	9.79 ± 0.20 ^a	8.33 ± 0.16 ^b	6.79 ± 0.09 ^c
Specific growth rate d ⁻¹	ZrCl ₄	0.28 ± 10 ^{-4a}	0.28 ± 10 ^{-3a}	0.28 ± 10 ^{-3a}	0.20 ± 10 ^{-3b}	0.14 ± 10 ^{-3c}	0.11 ± 10 ^{-3d}
	NPs-ZrO ₂	0.28 ± 10 ^{-4a}	0.28 ± 10 ^{-4a}	0.28 ± 10 ^{-3a}	0.27 ± 10 ^{-3a}	0.25 ± 10 ^{-3b}	0.21 ± 10 ^{-3c}
Growth inhibition %	ZrCl ₄	0 ± 0 ^a	0.4 ± 0.2 ^a	2.4 ± 1.5 ^b	29.8 ± 2.6 ^c	50.1 ± 1.6 ^d	59 ± 3.3 ^d
	NPs-ZrO ₂	0 ± 0 ^a	0.9 ± 1 ^a	1.7 ± 1.6 ^a	6.1 ± 2.1 ^b	10.8 ± 1.1 ^c	24.7 ± 1.8 ^d
Cyt-ROS level % of control	ZrCl ₄	100 ± 0 ^a	104 ± 1 ^b	106 ± 4 ^b	139 ± 4 ^c	126 ± 3 ^d	136 ± 6 ^c
	NPs-ZrO ₂	100 ± 0 ^a	104 ± 3 ^a	105 ± 5 ^a	115 ± 6 ^b	115 ± 8 ^b	125 ± 15 ^c
Org-ROS level % of control	ZrCl ₄	100 ± 0 ^a	108 ± 1 ^b	142 ± 1 ^c	157 ± 3 ^d	163 ± 1 ^e	171 ± 3 ^f
	NPs-ZrO ₂	100 ± 0 ^a	105 ± 2 ^b	107 ± 4 ^b	114 ± 7 ^b	122 ± 14 ^c	128 ± 20 ^c
Total thiols µmol/g DW	ZrCl ₄	12.65 ± 0.99 ^a	13.51 ± 0.45 ^a	16.75 ± 2.45 ^b	18.34 ± 1.66 ^b	19.47 ± 2.02 ^c	19.17 ± 1.50 ^c
	NPs-ZrO ₂	12.39 ± 1.30 ^a	17.20 ± 1.71 ^b	23.89 ± 1.72 ^c	29.83 ± 3.53 ^d	31.92 ± 1.49 ^d	31.85 ± 2.68 ^d

DW: dry weight; Cyt: cytoplasmic; Org: organites. The data represents the means of 3 replicates with 2 experimental sets (n = 6) for each parameter. Different letters are used to indicate significant differences between the control and the treatment concentrations at a significance level of $p < 0.05$.

Based on the results presented in Table 4, there are clear differences in how ZrCl₄ and NPs-ZrO₂ affect the biological parameters of *L. minor* plants in relation to Zr bioaccumulation. ZrCl₄ exposure led to significantly higher Zr bioaccumulation compared to the NPs-ZrO₂ at all concentrations tested. The bioaccumulation increased in a concentration-dependent manner for ZrCl₄, reaching 14.89 µg Zr/mg DW at 200 mg/L. In contrast, the bioaccumulation remained low for the NPs-ZrO₂, with a maximum of 0.04 µg Zr/mg DW at 200 mg/L. When *L. minor* plants were exposed to increasing concentrations of ZrCl₄ and the NPs-ZrO₂ for 7 days, the results revealed a proportional increase in plant growth inhibition with the bioaccumulation of Zr in the biomass. The bioaccumulation of Zr at a concentration of 13.63 µg/mg DW led to a growth inhibition of 50.1%, accompanied by a decrease in biomass. At low Zr concentrations (0.11 to 2.86 µg/mg DW), no significant variation in growth was noted. However, at higher concentrations (6.50 to 14.89 µg/mg DW), substantial growth inhibition occurred, ranging from 29.8% to 59.0%. This suggests that Zr ions have the potential to be highly toxic to the plant and accumulate in various organelles. Therefore, exposure to ZrCl₄ caused significant reductions in plant biomass and growth at nominal concentrations ≥ 50 mg/L, while exposure to the NPs-ZrO₂ only caused significant effects at ≥ 100 mg/L.

The effective concentration inhibiting half of the plant growth (EC50) could only be determined for growth parameters (biomass, specific growth rate, and growth inhibition) in *L. minor* exposed to ZrCl₄. The EC50 for these parameters was 58.69 mg/L of ZrCl₄, corresponding to a Zr bioaccumulation of 13.63 µg/mg DW. In comparison, the NPs-ZrO₂ exhibited a growth inhibition of 24.7% at the highest concentration tested, thus the EC50 values for growth parameters were higher than 200 mg/L. In addition, the data provided was insufficient to determine the EC50 values for oxidative stress markers (cytoplasmic and organelle ROS levels) and antioxidant responses (total thiols) for both ZrCl₄ and NPs-ZrO₂. However, these parameters were considered sensitive biomarkers for assessing the toxicity of ZrCl₄ and NPs-ZrO₂ in *L. minor* plants under the tested concentrations.

It is well known that oxidative stress plays a major role in the toxicity of metals and nanoparticles to plants, and the production of a high level of ROS can damage cellular components (proteins, lipids, and nucleic acids) contributing to the deterioration of the cellular physiology and plant growth [10,16,27,28,39,40]. Both cytoplasmic and organelle reactive oxygen species (ROS) levels increased with increasing concentrations of ZrCl₄

and the NPs-ZrO₂, indicating an oxidative stress effect in *L. minor* plants. However, exposure to ZrCl₄ generally induced higher ROS levels than the NPs-ZrO₂ under the same concentrations, which aligned with the higher bioaccumulation observed for ZrCl₄. To counteract oxidative stress, plants have evolved efficient defense mechanisms, including antioxidant enzymes and low molecular weight antioxidants like glutathione (GSH) [41,42]. In this study, the total thiol levels, an indicator of GSH content, exhibited a concentration-dependent increase in response to both ZrCl₄ and NPs-ZrO₂. Interestingly, despite the lower bioaccumulation and oxidative stress induced by the NPs-ZrO₂, they led to a more pronounced increase in total thiols compared to ZrCl₄. This could explain the lower inhibition in plant growth caused by the NPs-ZrO₂ when compared to ZrCl₄, suggesting that the NPs-ZrO₂ triggered a stronger antioxidant response in *L. minor* plants.

Several toxicological endpoints correlated with Zr toxicity have been determined in previous studies on different species of microalgae and plants, highlighting the potential ecological impact on aquatic ecosystems: 1. Significant changes in antioxidant enzyme activities, chlorophyll content, and biomass growth were observed for different plant species in Zr-contaminated soil [10,11]; 2. Zr-contaminated culture medium in aquaria caused a reduction in the biofilm biomass of different periphyton microorganism species [13]; 3. Nano-zirconium oxide (nZrO₂) affected the growth, mitochondria-generated ROS levels, and cellular membrane permeability of the freshwater alga *Chlorella pyrenoidosa* [16]; 4. In the unicellular freshwater alga *Scenedesmus obliquus* exposed to NPs-ZrO₂, several biological parameters were significantly altered, including ROS level, chlorophyll content, mitochondrial membrane potential, cellular membrane permeability, and antioxidant enzyme activity [25]; 5. The nZrO₂ was found to inhibit the growth of the microalga *Chlorella* sp. [43]. These findings demonstrate the need for further research to better understand the mechanisms of Zr toxicity in aquatic ecosystems, particularly its impact on primary producers such as microalgae and plants, which form the foundation of aquatic food webs. In our study, we determined that the correlations between Zr concentration, bioaccumulation, and toxic effects on *L. minor* plants were dependent on the chemical nature and properties of the Zr-compound. The obtained results show that the higher Zr bioaccumulation in plants exposed to ZrCl₄ was correlated with more severe effects on growth parameters and oxidative stress markers compared to exposure to NPs-ZrO₂. However, NPs-ZrO₂ induced a stronger antioxidant response despite lower bioaccumulation, emphasizing the complex interactions between this Zr-compound and the biological system of *L. minor*. This investigation demonstrated the importance of growth biomarkers and oxidative stress indicators in assessing the toxicity of ZrCl₄ and NPs-ZrO₂. Therefore, these findings contribute to a comprehensive understanding of the toxicity mechanisms and potential ecological impacts of these Zr-compounds.

Moreover, we identified the lowest nominal exposure concentration and the lowest observed effect dose (LOED) for both Zr-compounds causing a statistically significant effect on the toxicity biomarker compared to the control (Table 5). Based on these results, the most sensitive responses to the lowest nominal exposure concentration of ZrCl₄ were the Cyt-ROS and the Org-ROS, having the lowest LOED when compared to the other biological parameters. On the other hand, the most sensitive responses to the lowest nominal exposure concentration of the NPs-ZrO₂ were the Total thiols and the Org-ROS, although LOEDs were similar for all biological parameters. Therefore, the oxidative stress markers (cytoplasmic and organelle ROS) were among the most sensitive parameters for both Zr-compounds.

Table 5. The nominal exposure concentration (mg/L) and the lowest observed-effect dose (LOED) of $ZrCl_4$ and NPs- ZrO_2 for each biological parameter in *Lemna minor*. The LOED is expressed in $\mu\text{g}/\text{mg}$ dry weight (DW).

Biological Parameter	[$ZrCl_4$] mg/L	$ZrCl_4$ LOED $\mu\text{g Zr}/\text{mg DW}$	[NPs- ZrO_2] mg/L	NPs- ZrO_2 LOED $\mu\text{g Zr}/\text{mg DW}$
Growth Inhibition	50	2.86	100	0.01
Cyt-ROS	1	0.11	100	0.01
Org-ROS	1	0.11	1	0.01
Total Thiols	50	2.86	1	0.01

DW: dry weight; Cyt: cytoplasmic; Org: organites.

3.3. Impact of NPs- ZrO_2 on Plant Fronds and Roots

In this study, we investigated the impact of NPs- ZrO_2 on both the fronds and roots of the aquatic plant *Lemna minor*. Our scanning electron microscopy (SEM) observations revealed the adherence of NPs- ZrO_2 to the ultrastructures of the fronds and roots after 7 days of exposure (Figure 1). The unexposed control fronds and roots displayed a smooth, intact surface with no visible damage, featuring well-arranged and closely spaced cells. In contrast, the fronds and roots exposed to the NPs- ZrO_2 exhibited ultrastructural defects, including deep cracks and agglomerated NPs- ZrO_2 on the outer surface (Figure 1). These nanoparticle aggregates varied in size, ranging from small particles of 60 nm to larger particles of 1.05 μm . Therefore, these results clearly showed the detrimental effects of NPs- ZrO_2 exposure on *L. minor* fronds and roots compared to the healthy control plants. The nanoparticles caused visible damage to the frond surface and edges, while inhibiting root growth, and altering root morphology. Furthermore, the SEM observations coupled with energy dispersive X-ray spectroscopy (EDS) confirmed the presence of free Zr ions after the dissolution of the NPs- ZrO_2 , and this could explain the decrease in Zr content in the observed aggregates. The presence of Zr peaks in the EDS spectra of the exposed tissues, which are absent in the control, confirmed the internalization of the nanoparticles by the plant (Figure 2). This indicated the adhesion of the NPs- ZrO_2 to the ultrastructure of the fronds and roots of the *L. minor* plant and the subsequent Zr uptake. The uptake of Zr ions by the roots was evident, with aggregates containing high Zr concentrations detected on the root cell wall. This suggests that the released NPs- ZrO_2 and Zr ions can be absorbed by root cells and translocated to the fronds. Similar aggregates were observed at the frond level, with a Zr content of approximately 10–12% (Figure 2). The lower proportion of Zr in the fronds compared to the roots indicates that roots have a higher affinity for absorbing NPs- ZrO_2 and free Zr ions. The dissolution of the NPs- ZrO_2 during processing and the uptake of free Zr ions by the plant through the roots could explain the decrease in Zr content in the observed aggregates. A previous study provided a similar explanation for the toxicity of cerium oxide nanoparticles (NPs- CeO_2) in *Lemna minor* [44]. The authors revealed by SEM analysis that the frond stomata morphology was altered and that the root was responsible for Ce uptake. By using X-ray absorption near-edge structure (XANES) spectroscopy, their results confirmed the transformation of Ce from Ce(IV) to Ce(III) in duckweed treated with NPs- CeO_2 , suggesting that the toxicity of nanoparticles was mainly from the release of Ce ions. Therefore, our investigation provided valuable insights on the uptake mechanism of NPs- ZrO_2 , in addition to their incorporation and toxicity on the *L. minor* plant system.

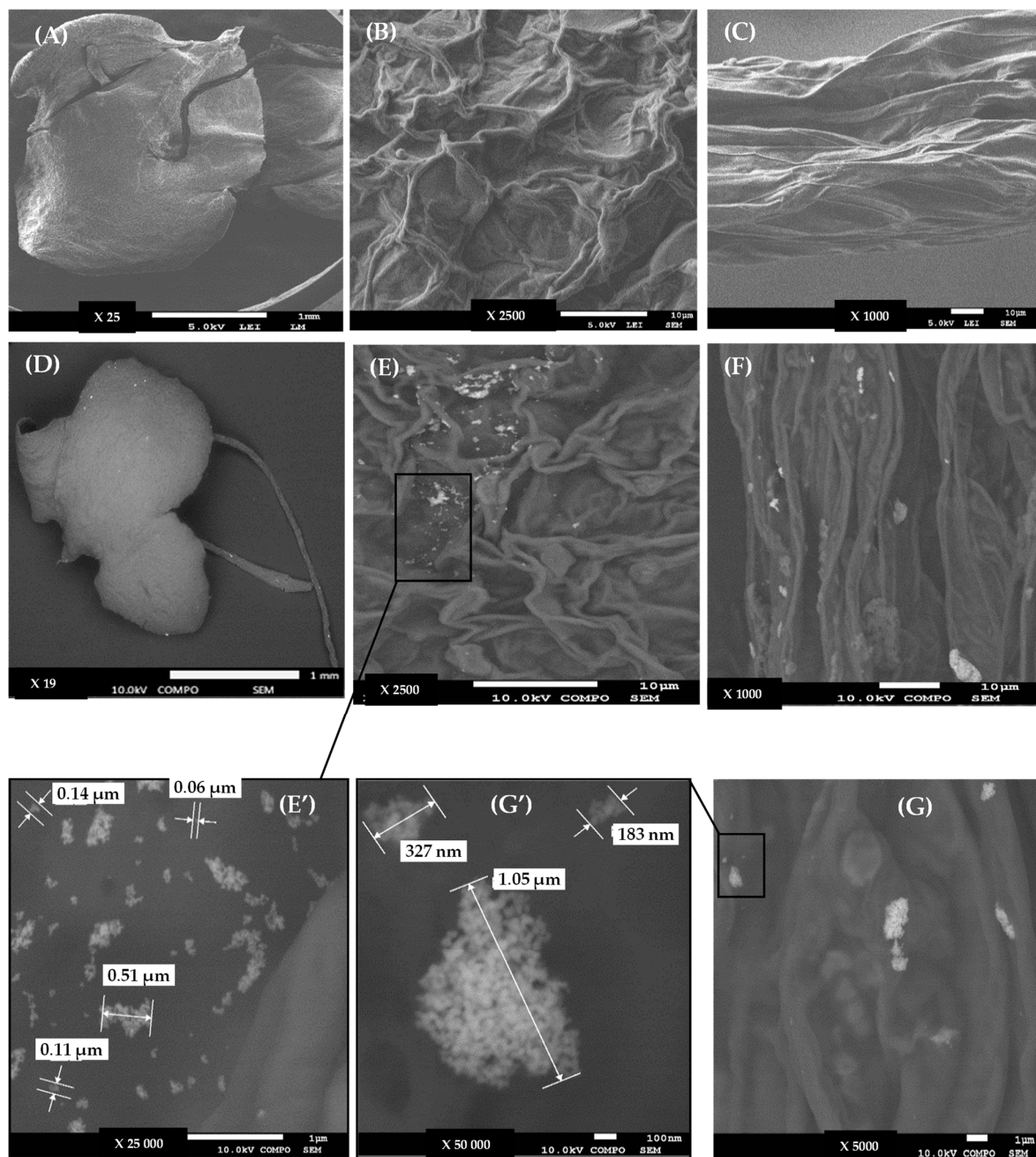


Figure 1. Scanning electron microscopy (SEM) images of *Lemna minor*, including the frond and root structures, under different conditions: (A–C), Control; (D–G), 7-day exposure to NPs-ZrO₂ under effective concentration for growth (100 mg/L). The images show the change in the plant frond and root structures under treatment with NPs-ZrO₂ when compared to the control: Image (A) shows a healthy frond with a smooth surface and no visible damage; Image (B) provides a closer view of the frond edge, which appears intact; In image (C), the root structure looks normal with fine root hairs extending from the main root; Image (D) depicts a frond with visible surface damage and abnormalities compared to the control, and the frond edges appear crumpled and irregular; A magnified view of the damaged frond edge is seen in image (E), showing a rough, uneven surface likely due to the effect of NPs-ZrO₂; In images (F,G), the root structures after NPs-ZrO₂ appear thicker and shorter with fewer fine root hairs compared to the control condition, suggesting that NPs-ZrO₂ negatively impact root growth and development. Frames (E',G') provide detailed views at a higher resolution of specific areas highlighted in images (E',G'), respectively. These magnified sections indicate that NPs-ZrO₂ have deposited on the surface.

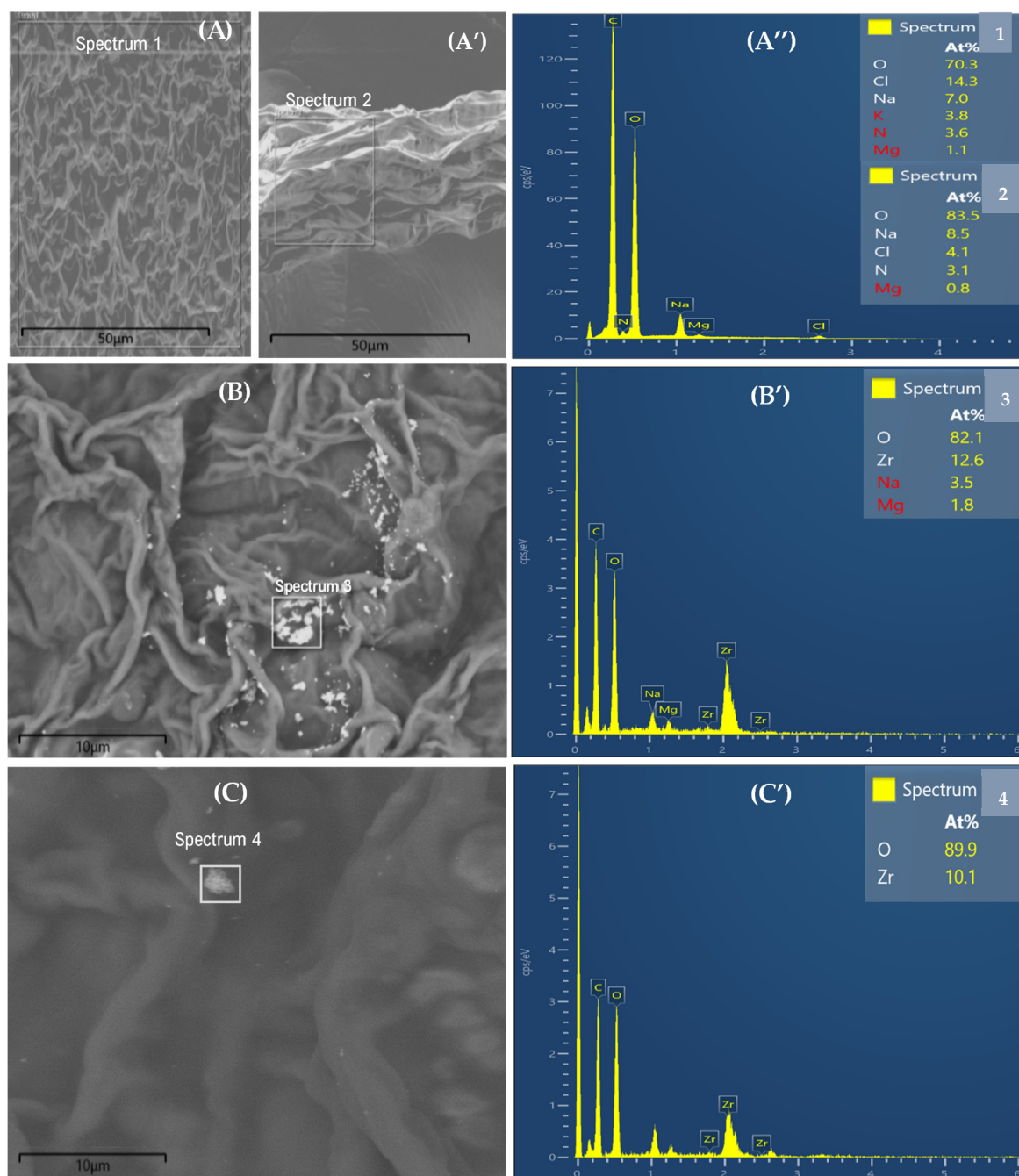


Figure 2. Energy-dispersive X-ray spectroscopy (EDS) coupled with scanning electron microscopy (SEM) images of *Lemna minor* plants: (A), control fronds; (B), 7-day exposed fronds to 100 mg/L of NPs-ZrO₂; (C), 7-day exposed roots. The images (A', B', C') show the elemental analysis of the plant tissues. In images (A, A'), the EDS spectrum of the control frond likely displays peaks for elements typically found in plant tissues, such as carbon, oxygen, and trace minerals (no Zr peak is expected in the control spectrum, since the plant was not exposed to NPs-ZrO₂); In image (B), when compared to the control, the EDS spectrum of the exposed frond shows an additional peak for Zr, indicating the uptake and accumulation of NPs-ZrO₂ in the frond tissues during the exposure period; In image (C), the EDS spectrum of the exposed root displays a Zr peak, confirming the presence of NPs-ZrO₂ in the root tissues. The intensity of the Zr peak in the root may differ from that in the frond, suggesting differential accumulation of NPs-ZrO₂ in various plant parts.

3.4. Ecological Implications of Zirconium Contamination in Aquatic Ecosystems

In this study, we showed the importance of considering the chemical speciation and transformation of Zr-compounds in aquatic environments. The formation of $\text{Zr}(\text{OH})_4(\text{aq})$ from ZrCl_4 and the dynamic behavior of NPs- ZrO_2 highlighted the necessity for comprehensive environmental fate and transport studies to predict the bioavailability and potential toxicity impacts of Zr-compounds under varying environmental conditions. Such information is crucial for regulatory agencies and policymakers when establishing guidelines for permissible Zr levels in water bodies. In addition, this study explored the differential toxicity mechanisms and potential ecological impacts of both ZrCl_4 and NPs- ZrO_2 on the aquatic plant *Lemna minor*, serving as a bioindicator species. Our findings indicated that these Zr-compounds exhibited distinct toxicity mechanisms due to their unique physicochemical properties. ZrCl_4 demonstrated higher toxicity, with its impact largely dependent on its concentration and bioavailability. In contrast, the NPs- ZrO_2 exhibited moderate toxicity, primarily due to its low solubility and sedimentation in aquatic environments, limiting its availability to plants. Additionally, the obtained results demonstrated the role of ROS levels and total thiols in the plant response to Zr toxicity, which significantly affected the health status of *L. minor*.

From an ecological standpoint, the differential bioaccumulation and toxicity of ZrCl_4 and NPs- ZrO_2 to *L. minor* have significant implications for aquatic ecosystems. As a primary producer, the aquatic plant *L. minor* plays a crucial role in nutrient cycling, food web dynamics, and habitat provision in freshwater environments. Disruption of *L. minor* growth and physiology due to Zr-compounds exposure can cascade through the ecosystem, affecting the functioning of the overall ecosystem. The bioaccumulation of Zr-compounds in aquatic plants such as *L. minor* raises concerns about trophic transfer and potential biomagnification in aquatic food chains. Zr that has accumulated in plant tissues may be consumed by herbivores and transferred to higher trophic levels, posing a risk to the entire ecosystem. This emphasizes the need for monitoring and management strategies to address the transfer of Zr contaminants from aquatic plants to higher trophic levels. On the other hand, the ability of *L. minor* to bioaccumulate Zr could be leveraged in phytoremediation efforts to mitigate water pollution and prevent the impact of toxicity on aquatic ecosystems.

In summary, our findings emphasize the importance of considering the physicochemical properties and toxicity of ZrCl_4 and NPs- ZrO_2 when assessing their environmental impact. Future studies should examine the effects of environmental parameters (e.g., pH, temperature, chemical interaction) on the physicochemical properties and toxicity of Zr-species for a more comprehensive understanding. In addition, future research should focus on investigating the long-term effects, trophic transfer, and ecosystem-level impacts of Zr-compounds to develop effective risk assessment and management strategies for protecting aquatic ecosystems.

Supplementary Materials: The following supporting information can be downloaded at: <https://www.mdpi.com/article/10.3390/environments11100222/s1>, Figure S1: Transmission electron microscopic (TEM) and energy dispersive X-ray spectroscopy (EDS) analyses of zirconium oxide nanoparticles (NPs- ZrO_2); Figure S2: X-ray diffraction (XRD) analysis of zirconium oxide nanoparticles (NPs- ZrO_2) determined the crystalline state of nanoparticles (NPs); Figure S3: The Raman spectrum of zirconium oxide nanoparticles (NPs- ZrO_2); Figure S4: The FT-IR (Fourier Transform Infrared) spectrum of ZrO_2 nanoparticles (NPs- ZrO_2) suspension in aqueous solution, providing insights into the functional groups and chemical bonds.

Author Contributions: Conceptualization, M.D. and D.D.; methodology, M.D. and D.D.; software, M.D.; validation, M.D. and D.D.; formal analysis, M.D. and D.D.; data curation, M.D. and D.D.; writing—original draft preparation, M.D. and D.D.; writing—review and editing, M.D. and D.D.; supervision, D.D. All authors have read and agreed to the published version of the manuscript.

Funding: This research received no external funding.

Institutional Review Board Statement: Not applicable.

Informed Consent Statement: Not applicable.

Data Availability Statement: The data generated during this study can be obtained upon request to the corresponding author.

Acknowledgments: The authors gratefully acknowledge the financial support provided by the Department of Chemistry to David Dewez, which facilitated the execution of this research. We extend our sincere appreciation to Andrew Rose, an undergraduate research trainee, for his technical assistance. The authors also express their gratitude to the technical staff at the Centre for Materials Characterization (CM2) of the École Polytechnique de Montréal for their expertise and support in conducting the scanning electron microscopy and energy-dispersive X-ray spectroscopy analyses.

Conflicts of Interest: The authors declare no conflicts of interest.

References

1. U.S. Geological Survey. *Mineral Commodity Summaries 2023*; U.S. Geological Survey: Reston, VA, USA, 2023; 210p.
2. Zhu, X.; Geng, Y.; Gao, Z.; Houssini, K. Investigating zirconium flows and stocks in China: A dynamic material flow analysis. *Resour. Policy* **2023**, *80*, 103139. [[CrossRef](#)]
3. Kalavathi, V.; Bhuyan, R.K. A detailed study on zirconium and its applications in manufacturing processes with combinations of other metals, oxides, and alloys—A review. *Mater. Today Proc.* **2019**, *19*, 781–786. [[CrossRef](#)]
4. Sutherland, R.C. Development of Zirconium for Use in the Chemical Processing Industry. In *Zirconium in the Nuclear Industry: 20th International Symposium*; Yagnik, S.K., Preuss, M., Eds.; ASTM International: West Conshohocken, PA, USA, 2023; 22p.
5. Chitoria, A.K.; Mir, A.; Shah, M.A. A review of ZrO₂ nanoparticles applications and recent advancements. *Ceram. Int.* **2023**, *49*, 32343–32358. [[CrossRef](#)]
6. Kroll, W. La production industrielle du titane et du zirconium malléables. *Rev. Métallurgie* **1950**, *47*, 1–18. [[CrossRef](#)]
7. Bora, U. Zirconium tetrachloride. *Synlett* **2003**, *2003*, 1073–1074. [[CrossRef](#)]
8. Nikoofar, K.; Khademi, Z. A review on green Lewis acids: Zirconium (IV) oxydichloride octahydrate (ZrOCl₂·8H₂O) and zirconium (IV) tetrachloride (ZrCl₄) in organic chemistry. *Res. Chem. Intermed.* **2016**, *42*, 3929–3977. [[CrossRef](#)]
9. Delongea, J.; Burnel, D.; Netter, P.; Grignon, M.; Mur, J.; Royer, R.; Grignon, G. Toxicity and pharmacokinetics of zirconium oxychloride in mice and rats. *J. Pharmacol.* **1983**, *14*, 437–447.
10. Shahid, M.; Ferrand, E.; Schreck, E.; Dumat, C. Behavior and impact of zirconium in the soil-plant system: Plant uptake and phytotoxicity. *Rev. Environ. Contam. Toxicol.* **2013**, *221*, 107–127.
11. Madany, M.M.Y.; AbdElgawad, H.; Galilah, D.A.; Khalil, A.M.A.; Saleh, A.M. Elevated CO₂ can improve the tolerance of *Avena sativa* to cope with zirconium pollution by enhancing ROS homeostasis. *Plants* **2023**, *12*, 3792. [[CrossRef](#)]
12. Smotraiev, R.; Nehrii, A.; Koltsova, E.; Anohina, A.; Sorochkina, K.; Ratnaweera, H. Comparison of wastewater coagulation efficiency of pre-polymerised zirconium and traditional aluminium coagulants. *J. Water Process Eng.* **2022**, *47*, 102827. [[CrossRef](#)]
13. Caroline, D.; Soizic, M.; Jacky, V.; Claude, F. Impact of zirconium on freshwater periphytic microorganisms. *Environments* **2019**, *6*, 111. [[CrossRef](#)]
14. Bellon, K.; Chaumont, D.; Stuerger, D. Flash synthesis of zirconia nanoparticles by microwave forced hydrolysis. *J. Mater. Res.* **2001**, *16*, 2619–2622. [[CrossRef](#)]
15. Soni, D.; Singh, J.; Kaurav, N.; Tripathi, J.; Sharma, A. Synthesis and characterization of zirconia nanocrystalline powder by thermal treatment method. *Mater. Today Proc.* **2022**, *54*, 908–911. [[CrossRef](#)]
16. Wang, Z.; Zhang, F.; Vijver, M.G.; Peijnenburg, W.J. Graphene nanoplatelets and reduced graphene oxide elevate the microalgal cytotoxicity of nano-zirconium oxide. *Chemosphere* **2021**, *276*, 130015. [[CrossRef](#)] [[PubMed](#)]
17. Bertrand, G.; Mévrel, R. Zirconia coatings realized by microwave plasma-enhanced chemical vapor deposition. *Thin Solid Film.* **1997**, *292*, 241–246. [[CrossRef](#)]
18. Nishizawa, K.; Miki, T.; Watanabe, E.; Taoda, H. Surface roughness control of zirconia films using a novel photoresponsive precursor molecule for improving its photocatalytic activity. *Mater. Sci. Forum* **2008**, *569*, 13–16. [[CrossRef](#)]
19. Zheng, H.; Liu, K.; Cao, H.; Zhang, X. L-Lysine-assisted synthesis of ZrO₂ nanocrystals and their application in photocatalysis. *J. Phys. Chem. C* **2009**, *113*, 18259–18263. [[CrossRef](#)]
20. Gremillard, L. *Biocéramiques: Des Monolithes aux Composites*; INSA de Lyon; Université Claude Bernard-Lyon I: Villeurbanne, France, 2009; 140p.
21. Hochella, M.F., Jr.; Mogk, D.W.; Ranville, J.; Allen, I.C.; Luther, G.W.; Marr, L.C.; McGrail, B.P.; Murayama, M.; Qafoku, N.P.; Rosso, K.M. Natural, incidental, and engineered nanomaterials and their impacts on the Earth system. *Science* **2019**, *363*, eaau8299. [[CrossRef](#)]
22. Glauser, S.; Astasov-Frauenhoffer, M.; Müller, J.A.; Fischer, J.; Waltimo, T.; Rohr, N. Bacterial colonization of resin composite cements: Influence of material composition and surface roughness. *Eur. J. Oral Sci.* **2017**, *125*, 294–302. [[CrossRef](#)]
23. Tabassum, N.; Kumar, D.; Verma, D.; Bohara, R.A.; Singh, M. Zirconium oxide (ZrO₂) nanoparticles from antibacterial activity to cytotoxicity: A next generation of multifunctional nanoparticles. *Mater. Today Commun.* **2021**, *26*, 102156. [[CrossRef](#)]

24. Sun, T.; Liu, X.; Zhan, X.; Ou, L.; Lai, R. Hepatic distribution and toxicity of zirconia nanoparticles in vivo and in vitro. *Process Saf. Environ. Prot.* **2021**, *147*, 134–145. [[CrossRef](#)]
25. Liu, Y.; Wang, S.; Wang, Z.; Ye, N.; Fang, H.; Wang, D. TiO₂, SiO₂ and ZrO₂ nanoparticles synergistically provoke cellular oxidative damage in freshwater microalgae. *Nanomaterials* **2018**, *8*, 95. [[CrossRef](#)] [[PubMed](#)]
26. Załęska-Radziwiłł, M.; Doskocz, N. Ecotoxicity of zirconium oxide nanoparticles in relation to aquatic invertebrates. *Desalination Water Treat.* **2015**, *57*, 1443–1450. [[CrossRef](#)]
27. Martinez, S.; Sáenz, M.; Alberdi, J.; di Marzio, W. Comparative ecotoxicity of single and binary mixtures exposures of cadmium and zinc on growth and biomarkers of *Lemna gibba*. *Ecotoxicology* **2020**, *29*, 571–583. [[CrossRef](#)] [[PubMed](#)]
28. Jmii, S.; Dewez, D. Toxic responses of palladium accumulation in duckweed (*Lemna minor*): Determination of biomarkers. *Environ. Toxicol. Chem.* **2021**, *40*, 1630–1638. [[CrossRef](#)]
29. Benghaffour, A.; Azzouz, A.; Dewez, D. Ecotoxicity of diazinon and atrazine mixtures after ozonation catalyzed by Na⁺ and Fe²⁺ exchanged montmorillonites on *Lemna minor*. *Molecules* **2023**, *28*, 6108. [[CrossRef](#)]
30. Al-Nabhan, E. Removal efficiency, accumulation and biochemical response of *Lemna minor* L. exposed to some heavy metals. *IOP Conf. Ser. Earth Environ. Sci.* **2022**, *1060*, 012037. [[CrossRef](#)]
31. Aslanzadeh, M.; Saboor, A.; Moradlou, O. Phytoremediation potential of duckweed (*Lemna minor* L.) for hexavalent chromium removal in synthetic wastewater: Unveiling physiological response and defense mechanisms against excessive heavy metal uptake. *Int. J. Environ. Sci. Technol.* **2024**. [[CrossRef](#)]
32. Sompura, Y.; Bhardwaj, S.; Selwal, G.; Soni, V.; Ashokkumar, K. Unrevealing the potential of aquatic macrophytes for phytoremediation in heavy metal-polluted wastewater. *J. Curr. Opin. Crop Sci.* **2024**, *5*, 48–61. [[CrossRef](#)]
33. Organisation for Economic Co-Operation and Development. *Lemna OECD Guidelines for the Testing of Chemicals. Test No. 221: Sp. Growth Inhibition Test*; OECD: Paris, France, 2006.
34. Mandavilli, B.S.; Janes, M.S. Detection of intracellular glutathione using ThiolTracker violet stain and fluorescence microscopy. *Curr. Protoc. Cytom.* **2010**, *53*, 9.35.1–9.35.8. [[CrossRef](#)]
35. Applerot, G.; Lellouche, J.; Lipovsky, A.; Nitzan, Y.; Lubart, R.; Gedanken, A.; Banin, E. Understanding the antibacterial mechanism of CuO nanoparticles: Revealing the route of induced oxidative stress. *Small* **2012**, *8*, 3326–3337. [[CrossRef](#)] [[PubMed](#)]
36. Canuel, E.; Vaz, C.; Matias, W.G.; Dewez, D. Interaction effect of EDTA, salinity, and oxide nanoparticles on alga *Chlamydomonas reinhardtii* and *Chlamydomonas euryale*. *Plants* **2021**, *10*, 2118. [[CrossRef](#)] [[PubMed](#)]
37. Sharan, A.; Nara, S. Phytotoxic properties of zinc and cobalt oxide nanoparticles in algae. In *Nanomaterials in Plants, Algae and Microorganisms: Concepts and Controversies: Volume 2*; Academic Press: Amsterdam, The Netherlands, 2018; pp. 1–22.
38. Gambardella, C.; Gallus, L.; Gatti, A.M.; Faimali, M.; Carbone, S.; Antisari, L.V.; Falugi, C.; Ferrando, S. Toxicity and transfer of metal oxide nanoparticles from microalgae to sea urchin larvae. *Chem. Ecol.* **2014**, *30*, 308–316. [[CrossRef](#)]
39. Bielmyer-Fraser, G.K.; Jarvis, T.A.; Lenihan, H.S.; Miller, R.J. Cellular partitioning of nanoparticulate versus dissolved metals in marine phytoplankton. *Environ. Sci. Technol.* **2014**, *48*, 13443–13450. [[CrossRef](#)]
40. Cuypers, A.; Hendrix, S.; Amaral dos Reis, R.; De Smet, S.; Deckers, J.; Gielen, H.; Jozefczak, M.; Loix, C.; Vercampt, H.; Vangronsveld, J. Hydrogen peroxide, signaling in disguise during metal phytotoxicity. *Front. Plant Sci.* **2016**, *7*, 470. [[CrossRef](#)]
41. Rajput, V.D.; Harish, Singh, R.K.; Verma, K.K.; Sharma, L.; Quiroz-Figueroa, F.R.; Meena, M.; Gour, V.S.; Minkina, T.; Sushkova, S.; et al. Recent developments in enzymatic antioxidant defence mechanism in plants with special reference to abiotic stress. *Biology* **2021**, *10*, 267. [[CrossRef](#)]
42. Koh, Y.S.; Wong, S.K.; Ismail, N.H.; Zengin, G.; Duangjai, A.; Saokaew, S.; Phisalprapa, P.; Tan, K.W.; Goh, B.H.; Tang, S.Y. Mitigation of environmental stress-impacts in plants: Role of sole and combinatory exogenous application of glutathione. *Front. Plant Sci.* **2021**, *12*, 791205. [[CrossRef](#)]
43. Fu, M.; Liang, J.; Wang, S.; Geng, C.; Zhang, W.; Wu, T. The response of microalgae *Chlorella* sp. to free and immobilized ZrO₂ and Mg(OH)₂ nanoparticles: Perspective from the growth characteristics. *Environ. Eng. Sci.* **2020**, *37*, 429–438. [[CrossRef](#)]
44. Liu, Y.; Zhao, X.; Ma, Y.; Dai, W.; Song, Z.; Wang, Y.; Shen, J.; He, X.; Yang, F.; Zhang, Z. Interaction of cerium oxide nanoparticles and ionic cerium with duckweed (*Lemna minor* L.): Uptake, distribution, and phytotoxicity. *Nanomaterials* **2023**, *13*, 2523. [[CrossRef](#)]

Disclaimer/Publisher’s Note: The statements, opinions and data contained in all publications are solely those of the individual author(s) and contributor(s) and not of MDPI and/or the editor(s). MDPI and/or the editor(s) disclaim responsibility for any injury to people or property resulting from any ideas, methods, instructions or products referred to in the content.